Olle Törnblom*

Turbulent Shear and Breakup of Flocculated Biomaterial in Centrifuge Inlets

Analyses and simulations of a lab-scale device for determining floc strength are presented together with simulations of two different hermetic disc-stack centrifuge inlets. Two methods for determining the turbulent shear stresses on flocs in hermetic centrifuge inlets are described. A model for the average shear rate in a hermetic centrifuge inlet is proposed. A correlation for estimating the floc size of the centrifuge feed after passing the high-shear zone of the inlet is derived.

Keywords: Biomaterial, Computational fluid dynamics, Disc-stack centrifuge, Flocculation, Turbulent shear

Received: June 08, 2018; *revised:* August 30, 2018; *accepted:* September 07, 2018

DOI: 10.1002/ceat.201800297

1 Introduction

There is an increasing interest in large-scale production of tailored chemicals from renewable resources. Such production typically involves a fermentation step where microorganisms produce the chemical of interest. The extraction of the chemical from the fermentation broth usually necessitates the removal of the microorganisms in a prior process step. In biomedical applications, centrifugal disc-stack separators of hermetic design are known to be well-suited for this removal step. However, the larger scale of the production of base chemicals puts new demands in terms of throughput and energy consumption on the fermentation technique to be competitive against the use of fossil resources.

The separation of microorganisms from fermentation broths becomes increasingly difficult with smaller size of the organisms. The possible throughput of a centrifugal separator is essentially proportional to the Stokes settling velocity of the particles that are to be separated; see, e.g., Ambler [1] or Axelsson and Madsen [2]. Agglomeration of the microorganisms into larger clusters, which have higher settling velocities, prior to separation can improve significantly the centrifuge's throughput. The agglomeration can be achieved by the addition of coagulants or flocculants to the fermentation broth before the separation. For this technique to be successful the agglomerates cannot break apart due to, e.g., shear forces in the inlet of the centrifuge. If single organisms break loose from the agglomerates, they are likely to pass through unseparated.

A method is presented for estimating the typical floc size of a suspension after it has passed through a hermetic centrifuge inlet. The shear stability of the flocs in lab scale is determined by subjecting a sample to known shear rates in a spinning disc device (SDD). The shear rates of the SDD are assessed through computational fluid dynamics (CFD) simulations. Knowing the shear rates of the SDD for different rotation speeds of the disc, the measured average floc sizes can be used for fitting the coefficients for a relation between floc size and shear rate. This relation can then be applied for estimating the floc size after a centrifuge inlet using inlet shear rates extracted from a CFD simulation of said inlet.

A centrifugés cut size in terms of the smallest Stokes velocity,

$$v_g = \frac{d_{floc}^2(\rho_{floc} - \rho)g}{18\mu} \tag{1}$$

of the flocs that are fully separated is related to its area equivalent Σ[1)] and the volumetric flow rate Q [2]:

$$v_g = \frac{Q}{\Sigma} \tag{2}$$

Combining Eqs. (1) and (2) shows that a centrifugés throughput is proportional to the squared floc size. This motivates the use of flocculation and the study of floc breakage in centrifuge inlets.

Centrifuge inlets (Fig. 1) can be divided into two major categories: open and hermetic. In the open inlet (Fig. 1 a) the feed stream is introduced through a stationary pipe mounted centrally in the separator rotor. Between the stationary inlet pipe and the rotating bowl components is an air-filled gap. The non-rotating liquid is brought into rotation as it meets the rotating bowl components and the spun-up liquid forms a cylindrical free surface in the inlet. The open inlet is mechanically simpler than its hermetic counterpart since it does not require seals between rotating and stationary parts.

The hermetic inlet (Fig. 1 b) involves a rotating feed pipe which requires a mechanical seal to be fitted at the interface to the feed line. Often the rotor shaft is bored to a hollow shaft used as feed pipe. An obvious advantage of the hermetic design is that

1) List of symbols at the end of the paper.

Dr. Olle Törnblom
olle.tornblom@alfalaval.com
Alfa Laval Tumba AB, Hans Stahles väg 7, 147 80 Tumba, Sweden.

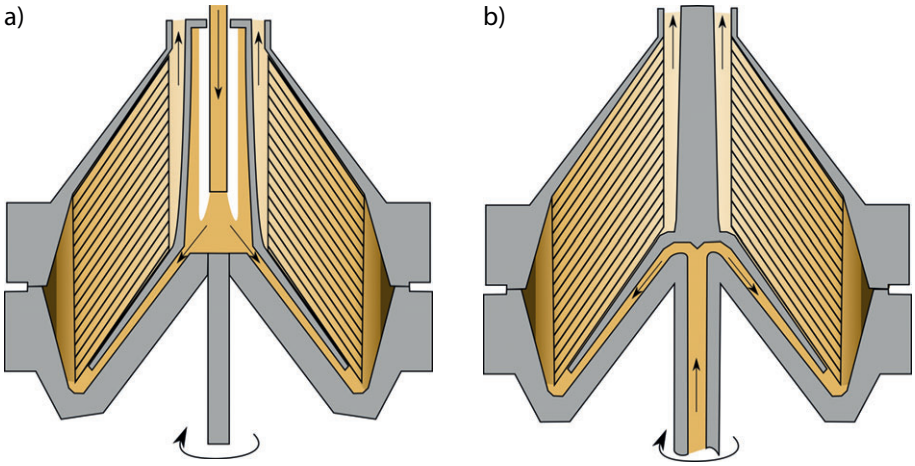

Figure 1. Sections of centrifuge bowls with open (a) and hermetic (b) inlets.

the feed never gets exposed to air or gas which can oxidize the product, cause foaming, or dissolve into the product. Another advantage is the reduced shear that the feed is subjected to.

Previous investigations by Boychyn et al. [3, 4] and Hutchinson et al. [5] confirm that the separability of biological material can be substantially reduced if the feed is subjected to strong shear stresses in the inlet. Hutchinson et al. [5] also described a large difference in separability of a cell culture that has passed through a hermetic inlet compared to one that is fed to the separator through a traditional open inlet. The observed difference is attributed to the lower shear forces in hermetic inlets.

Several different relationships for characterizing the strength of flocs have been suggested. Typically, these relationships correlate a characteristic size d of the flocs to the shear rate G of the liquid suspension. Many experiments on floc strength have been carried out by agitating a suspension using a rotating impeller [6]. Stirring a suspension of flocculating material long enough at constant impeller speed often results in an equilibrium floc average size, where there is a balance between the rates of floc breakage and floc formation due to colliding flocs or particles. Typically, the floc formation rate is reduced as the flocs grow and the probability of collisions decreases, while the rate of floc breakage typically increases with size.

The way flocs do break varies, and two distinctly different behaviors can be identified: erosion and large-scale fragmentation [6]. Erosion means that small fragments break away from the floc surface, causing a long tail of the size distribution towards small diameters. In large-scale fragmentation the flocs split into smaller flocs of similar size. Large-scale fragmentation leads to a shift in floc size distribution towards smaller sizes. Which one of the two behaviors dominates depends on several circumstances such as turbulence length scales and compactness of the flocs [6].

The breakage of flocs and the breakage of liquid droplets in shear flows are governed by similar laws. Hinze [7] derived on theoretical grounds a correlation for the maximum droplet size, d_{max}, in a dilute emulsion subjected to turbulent flow. The correlation

$$d_{max} = C_b \left(\frac{\sigma}{\rho \varepsilon^{2/3}} \right)^{3/5} \tag{3}$$

relates the critical Weber number of droplets to the length and velocity scales in the energy cascade of homogeneous isotropic turbulence. In Eq. (3), σ is the surface tension between the two liquids, ρ is the density of the continuous liquid, and ε is the energy dissipation rate of the turbulence per unit mass. A similar relation for flocs, namely,

$$d_{floc} = C_f G_{avg}^{-\gamma} \tag{4}$$

was suggested in [8] based on empirical observations. The floc strength coefficient C_f and the stable floc size exponent γ can be fitted to measurement data. Larger values of C_f indicates stronger flocs and the value of γ can give an indication of the dominant mode of floc breakage. Large values of γ can be interpreted as sign of erosion-dominated breakage [6]. It should be noted that Eq. (4) does not meet the criteria of being dimensionally correct for arbitrary values of γ.

The flow in a centrifuge inlet of industrial scale is with few exceptions turbulent and the average shear rate G_{avg} is dominated by the shear caused by the turbulence. It is hence reasonable to use the relation

$$G_{avg} = \sqrt{\frac{\varepsilon_{avg}}{\nu}} \tag{5}$$

where ε_{avg} is the average turbulence dissipation rate and ν is the kinematic viscosity. Interestingly, Eq. (3) corresponds to a γ-value of 4/5 if using Eq. (5) to compare the relationship between diameters predicted by Eqs. (3) and (4). The turbulence dissipation rate can be extracted from CFD simulations of the lab-scale experiment and the centrifuge inlet. Eq. (5) can then be applied to estimate the shear in a lab-scale test of a flocculated suspension so that a fit of the constants C_f and γ in Eq. (4) can be made using measurements of d_{floc}. An estimate of the floc size after the centrifugés inlet can now be calculated by Eq. (4) and the average shear G_{avg} from the inlet simulation.

2 Numerical Models

Solutions for the steady-state flow in the SDD and in the inlet of a pilot-scale hermetic centrifuge inlet were achieved using the open source CFD toolbox OpenFOAM v5.0. The incompressible Reynolds-averaged Navier-Stokes (RANS) equations [9] were solved using a k-ω-SST [10] closure for the Reynolds stress term. The equations were discretized by the finite volume method (FVM) on an unstructured computational grid. A second-order accurate differencing scheme was used for the momentum equations and a first-order accurate upwind scheme was applied to the turbulence transport equations [11]. The discretized system of equations was solved in a segregated manner with the SIMPLEC algorithm [12].

The automatic near-wall treatment boundary condition of [13] was applied to ω on all solid walls, both rotating and stationary. A zero-gradient boundary condition was selected for the turbulence kinetic energy k.

2.1 Spinning Disc Device

The SDD was very similar to the device described by Levy et al. [14]. The core of the SDD was a cylindrical chamber of stainless steel with a rotating stainless-steel disc in the center; see Fig. 2. The chamber's inner diameter was 50 mm and the height 25 mm. The disc was integrated onto a 4-mm shaft, had a thickness of 1 mm and a diameter of 40 mm. Two holes with 2 mm diameter were located 180° apart in the lower part of the chamber. These holes can be used either to feed at continuous flow through the SDD or for filling and draining a batch sample. An electrical controller allows the SDD to be run at different speeds from 1000 to 20 000 rpm. By altering the rotation speed a wide range of shear rates can be achieved.

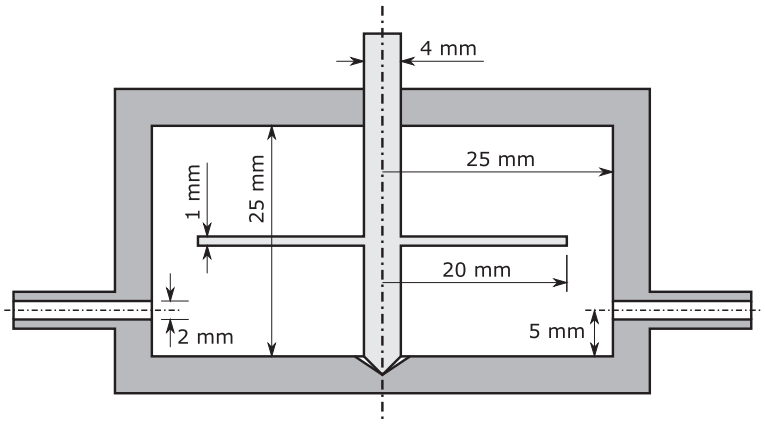

Figure 2. Spinning disc device with its main dimensions.

The SDD experiments were conducted on a fermentation broth containing *Corynebacterium glutamicum* microorganisms diluted 1:500 with demineralized water. The microorganisms had been inactivated by a heat treatment. *Corynebacterium glutamicum* are rod-shaped and 1–2 µm long. The concentration of microorganisms in the SDD experiments was 0.011–0.018 vol % of wet biomass. The flow through the SDD was 200 mL min^{-1} corresponding to an average residence time of 15 s. Batch tests with the SDD were performed in order to ascertain that this residence time was enough to reach a steady-state size distribution, and CFD simulations showed that all streamlines of the flow though the SDD were passing through the high-shear zone close to the spinning disc. The flocculant used was of polyvinylamine type (BASF Catiofast VFH) and was added to the broth at a concentration of 10 kg t^{-1}. Particle size distributions before and after the SDD were measured by laser diffraction with an inline Malvern Mastersizer 3000 (Malvern Instruments Ltd, UK). For further details on the experiments see Merkel et al. [15].

In the numerical simulations the SDD is modeled in a stationary reference frame. Since the rotating disc is axisymmetric, its velocity can be introduced as a moving-wall boundary condition. A constant through-flow of 200 mL min^{-1} was set on the inlet boundary and a constant pressure was applied on the outlet. The computational grid had 2.4 million mainly hexahedral cells and was refined near the wall boundaries to resolve the boundary layers. The height of the first cell was less than 4 µm on the rotating disc and less than 20 µm on the chamber walls. A section of the mesh is presented in Fig. 3.

2.2 Pilot-Scale Hermetic Inlet

The hermetic inlet is modeled in a reference frame rotating with the same speed as the centrifuge. The rotating frame formulation of the governing equations introduces two additional terms: the Coriolis force and the centrifugal force. In incompressible flow, the latter is balanced by a pressure gradient, and omitting the centrifugal force results in the reduced pressure formulation [16] of the equations, which was used in this investigation. The Coriolis force is introduced as an explicit body force.

The inlet geometry was derived from a CAD model of the pilot-scale centrifuge (Alfa Laval Explorer). The diameter of the inlet pipe was 14 mm and the total diametral extent of the CFD model was 120 mm. The computational grid had 2.2 million mainly tetrahedral and pentahedral cells. Layers of pentahedral cells were created to resolve the near-wall gradients. The first layer height was 10 µm. A section of the mesh is displayed in Fig. 4.

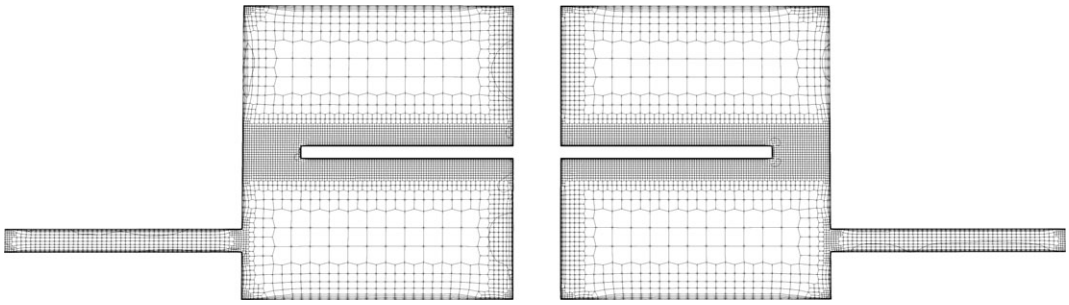

Figure 3. Section of the computational grid for the spinning disc device.

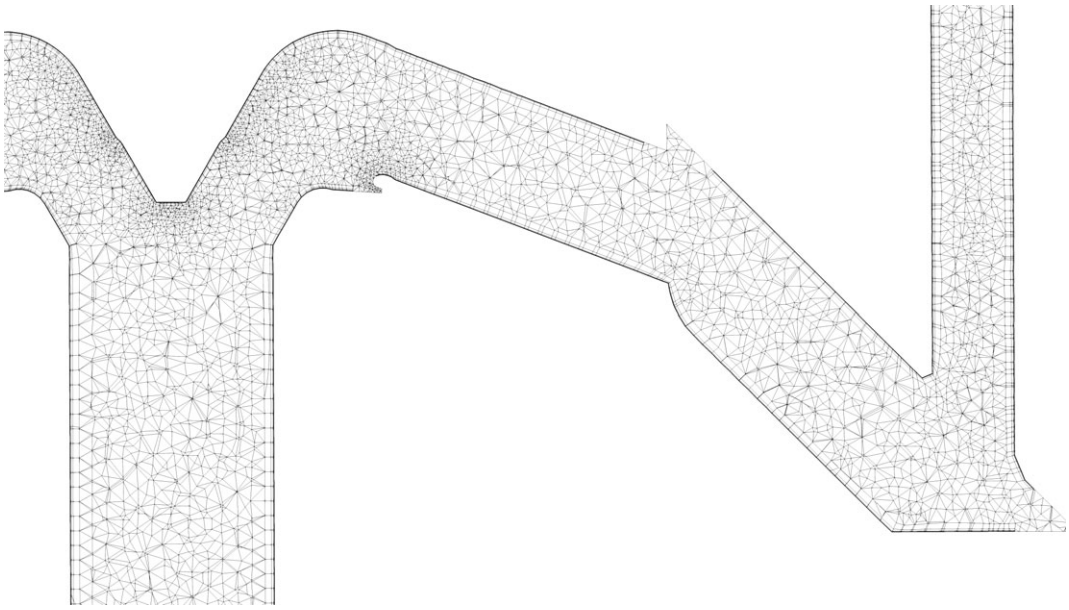

Figure 4. Section of the computational grid for the pilot-scale hermetic inlet.

2.3 Industrial-Scale Hermetic Inlet

The industrial-scale hermetic inlet was modeled in the same way as the pilot-scale inlet. The geometry was a generic large-size Alfa Laval centrifuge with a bowl outer diameter of approximately 800 mm. The inlet pipe was 44 mm in diameter and the total diameter of the model was 345 mm. The computational grid had 1.6 million tetrahedral and pentahedral cells. Near-wall gradients were resolved using layers of pentahedral cells. The first layer height was 50 μm. A section of the mesh is illustrated in Fig. 5.

3 Results and Discussion

The numerical models for the SDD and the two inlets were used for investigating how the rotation speed and flow rate influence both the local and the global shear rates. The simulated cases are summarized in Tab. 1.

Fig. 6 indicates the turbulence dissipation rate in a cross section of the pilot-scale inlet. The figure is included as an example of a typical flow in a hermetic inlet. Note that the color scale is logarithmic. The highest dissipation rates are found in small regions in the interface between the axisymmetric flow in the inlet pipe and the radially directed distributor channels. Also noticeable are the thin regions of high dissipation rate in the upper part of the distribution channels. The qualitative character of the flow is very similar in all simulations of the pilot-scale inlet.

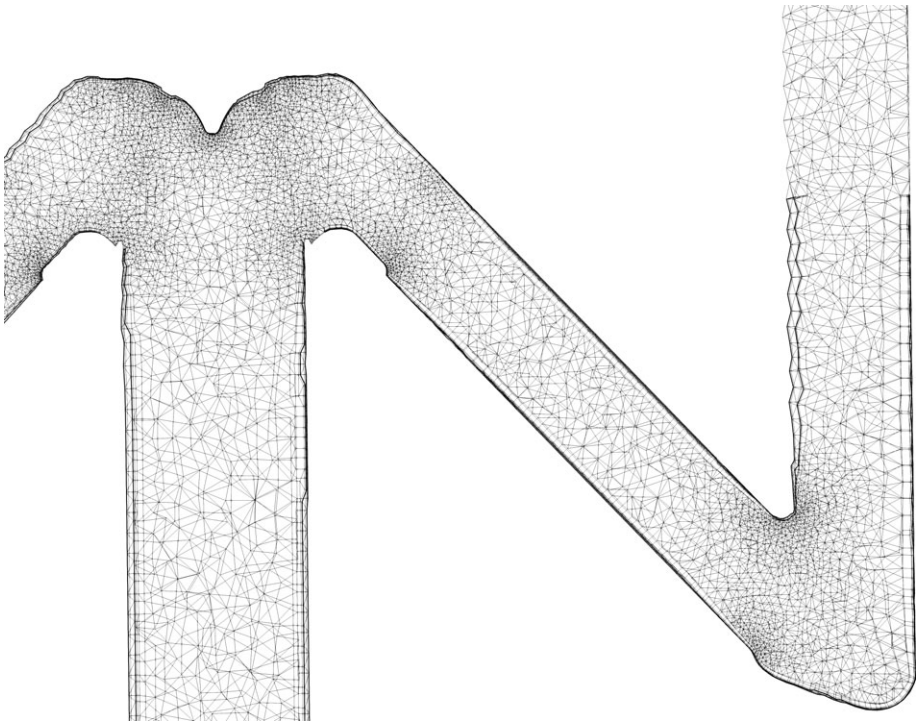

Figure 5. Section of the computational grid for the industry-scale hermetic inlet.

Table 1. Summary of simulated cases and comparison of averaged results.

Speed [rpm]	Flow rate [L h^{-1}]	ε_{avg} [m^{2}s^{-3}]	d_{avg} [µm]	ε_{median} [m^{2}s^{-3}]	d_m [µm]
SDD					
1 000	12	0.7	50.7	2	217
5 000	12	47	12.9	2200	13.2
10 000	12	303	7.0	9500	7.3
Pilot-scale inlet					
5 000	1 000	57	12.1	250	31.5
8 000	1 000	82	10.7	494	24.0
10 000	1 000	94	10.3	499	23.9
12 000	1 000	95	10.2		
10 000	500	22	16.5		
10 000	250	15	18.5		
Industry-scale inlet					
4 800	10 000	56	12.2		
4 800	30 000	262	7.3		
4 800	50 000	609	5.6		
4 800	70 000	1390	3.4		
4 800	90 000	2881	4.3		
4 800	110 000	5324	2.8		

3.1 Average Energy Dissipation Rates

The average dissipation rate ε_{avg} for the SDD was calculated as:

$$\varepsilon_{avg} = \frac{\tau\omega}{\rho V} \tag{6}$$

where τ is the torque of the rotating disc and shaft and ω is the angular velocity of the disc. The torque is a result of the flow simulation. The volume V was taken as the volume of the computational domain. A common way to calculate the average dissipation in a stirred-container experiment is to use the impeller power number N_p, the rotor speed n (in turns per second) and the impeller diameter D_i:

$$\varepsilon_{avg} = \frac{N_p n^3 D_i^5}{V} \tag{7}$$

The average power number for the simulated SDD cases was N_p = 0.04. Eq. (7) is useful for estimating ε_{avg} in the SDD without having to perform a CFD analysis.

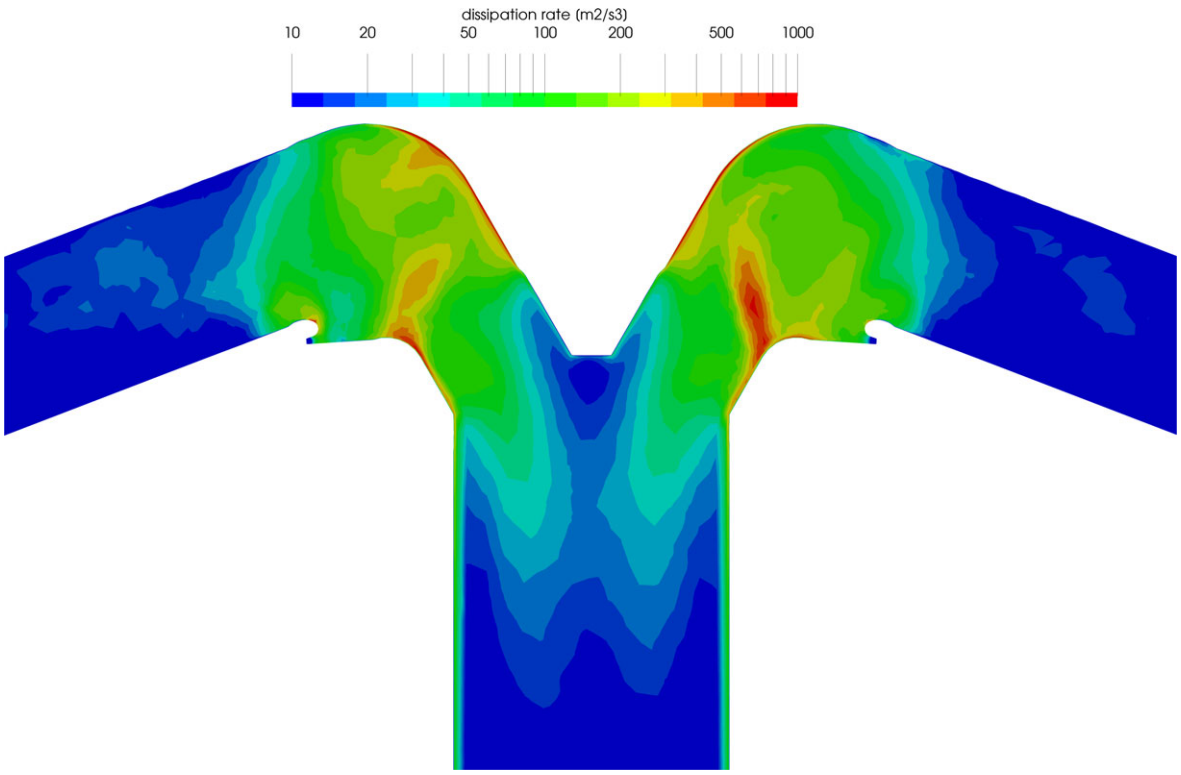

Figure 6. Contours of the turbulence dissipation rate in the pilot-scale inlet. Rotation speed 8000 rpm, flow rate 1000 L h^{-1}.

The average dissipation rate in the inlet geometries was calculated through the loss of total pressure between two sections before and after the zone of high shear in the inlet.

$$\varepsilon_{\mathrm{avg}} = \frac{Q(p_1 - p_2)}{\rho V} \tag{8}$$

The total pressures p_1 and p_2 were taken as the average values of $p + \frac{1}{2}\rho U^2$ where p is the reduced pressure (cf. [16]) and U is the magnitude of the velocity relative to the rotating frame of reference.

Using the results from the inlet simulations and dimension analysis, the correlation

$$\varepsilon_{\mathrm{avg}} = C_{\mathrm{inlet}} \frac{Q^2\omega}{D_{\mathrm{inlet}}^4} \tag{9}$$

was derived, where D_{inlet} is a length scale taken as the diameter of the inlet pipe. A value of 0.0338 for the coefficient C_{inlet} was found to give the best fit to the available data. Fig. 7 a shows $\varepsilon_{\mathrm{avg}}$ from the industry-scale inlet plotted against the flow rate together with the correlation in Eq. (9). It may be noted that the machines in the field operate throughout the measured range, but depending on the application they run either at the left-hand side, like for bacteria removal, or at the right-hand side of the range when separating, e.g., yeast. Fig. 7 b indicates $\varepsilon_{\mathrm{avg}}$ from the pilot-scale inlet plotted against the bowl speed together with the correlation in Eq. (9), and it is notable that the dissipation rate is markedly lower, by 1–2 orders of magnitude, than for the industrial-scale centrifuge.

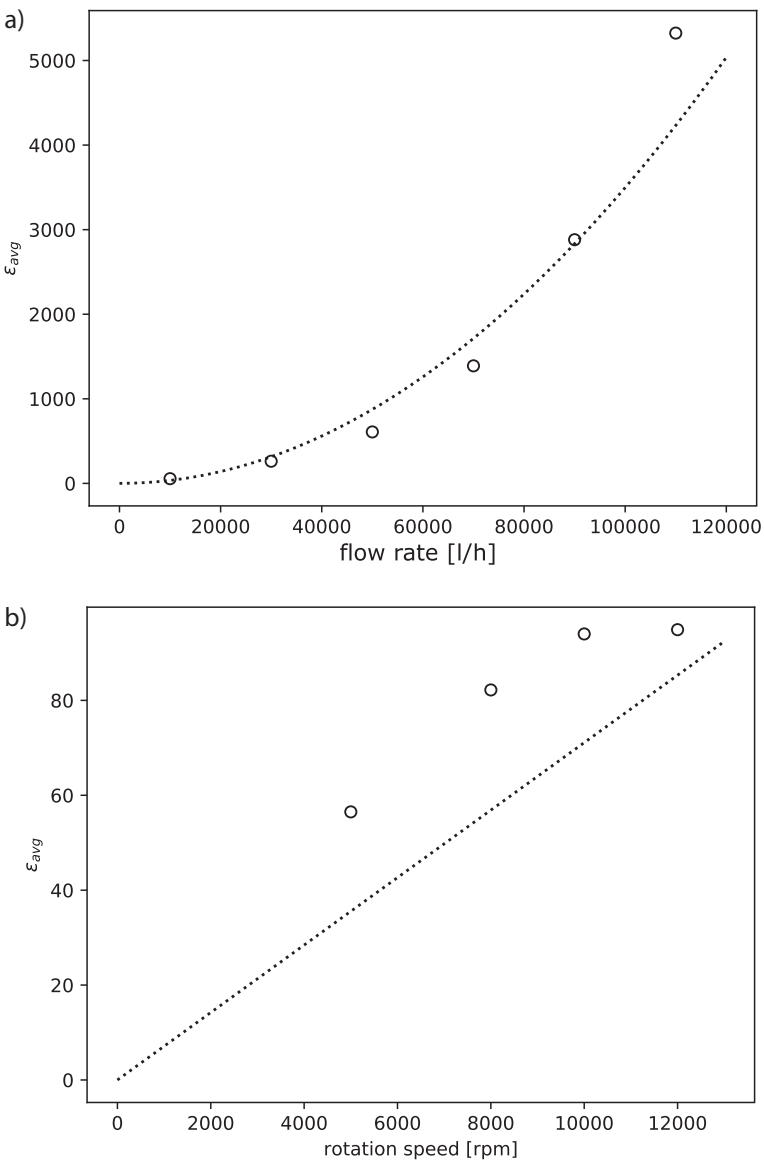

Figure 7. Average dissipation rate $\varepsilon_{\mathrm{avg}}$ for (a) pilot- and (b) industry-scale inlets (circles) and the correlation from Eq. (9).

3.2 Dissipation Rates from Streamline Analysis

Assuming that a floc will hold together if not subjected to shear stresses above its rupture strength, the application of the average dissipation rate will give an underestimation of the floc strength. An analysis of streamlines was done to investigate the relationship between average dissipation rate, or shear, and the distribution of shear forces that the feed stream encounters when passing the inlet. A large number of streamlines were tracked from the inlet pipe through the high-shear zone. The maximum value of the turbulent dissipation rate ε encountered by each streamline was detected. The resulting distribution for the probability at a certain maximum dissipation rate is illustrated in Fig. 8.

The median dissipation rate taken from the distributions in Fig. 8 is substantially larger than the volume average dissipation rate; see Tab. 1. For the SDD, the median is a factor 30–40 times larger and for the inlet the factor it is around 13.

3.3 Floc Strength

Fig. 9 demonstrates the laser diffraction measurements of the flocculated bacteria suspension processed through the SDD at various shear rates. Details on these measurements can be found in [15]. The median diameter of the distributions treated at 5000 and 10 000 rpm were used together with the $\varepsilon_{\mathrm{avg}}$ in Eq. (6) to fit the parameters in Eq. (4). This gave $C_{\mathrm{f}} = 4000$ and $\gamma = 0.65$ for diameters in µm. The fit is shown in Fig. 10, denominated as average shear. The fit is then used for calculating estimates of the median diameters in the simulated cases. The resulting floc diameters d_{avg} are listed in Tab. 1.

Fitting the parameters of Eq. (4) to the measurement data but instead using the median dissipation rates to estimate G results in a fit with $C_{\mathrm{f}} = 72\,000$ and $\gamma = 0.8$ for floc diame-

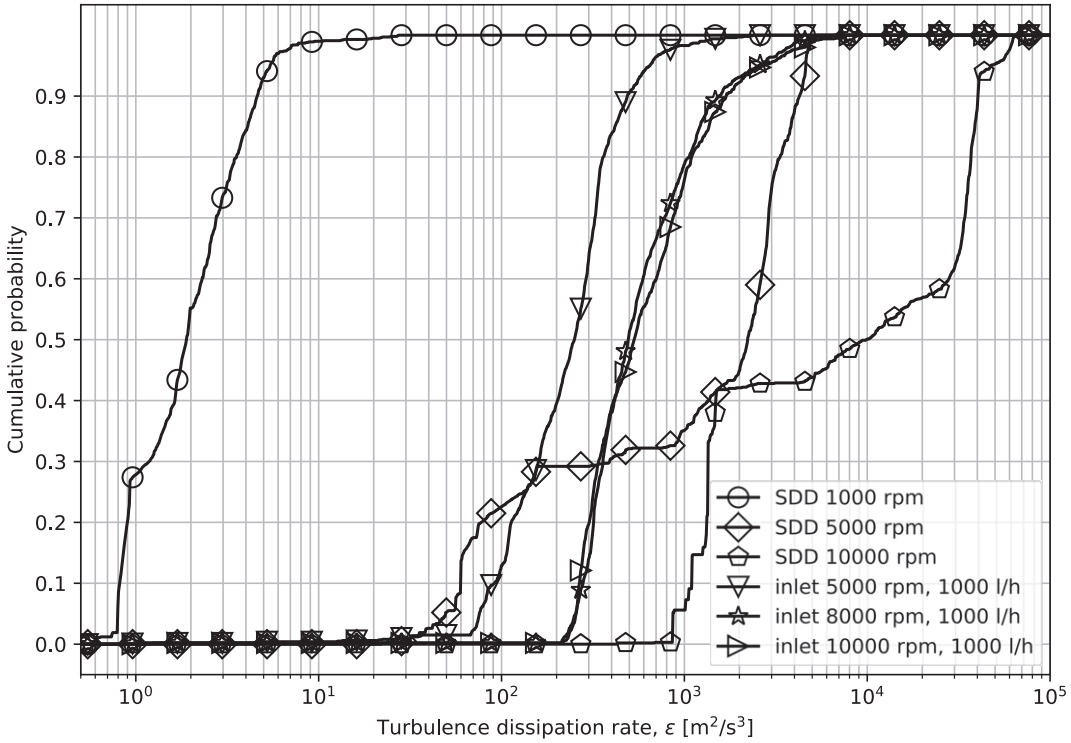

Figure 8. Cumulative distributions for the probability of a maximum dissipation rate along streamlines.

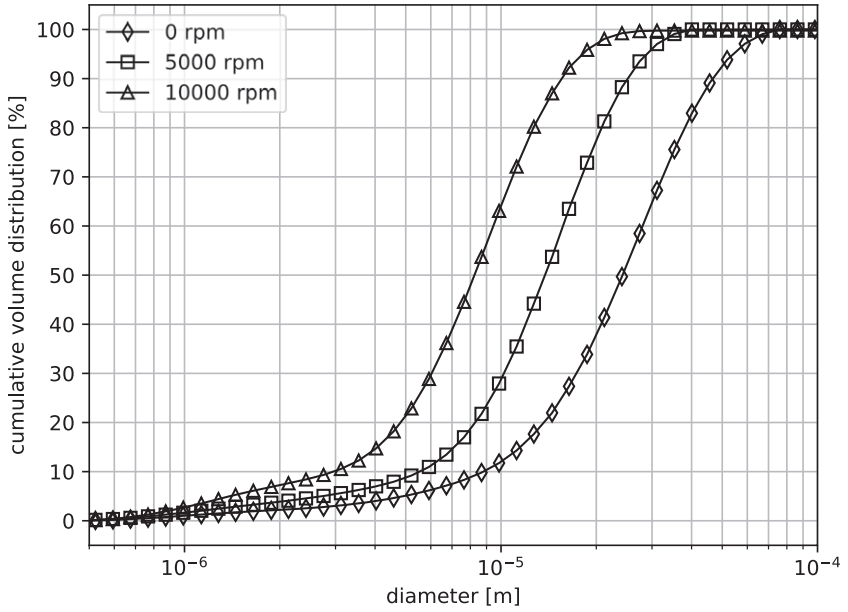

Figure 9. Laser diffraction measurements of bacteria flocs subjected to shear in the SDD at disc speeds of 0, 5000, and 10 000 rpm. Data from [15].

ters in µm. It can be noted that the value of γ is the same as that theoretically derived in [7]. The fit is denominated as median shear in Fig. 10. The resulting fit was employed for calculating the expected floc diameter d_m (calculated using the streamline median) for three cases of the pilot-scale inlet; see Tab. 1. The resulting diameters are larger than those predicted from the fit based on average shear rates, reflecting the difference between the SDD and the pilot-scale inlet in the relation $\varepsilon_{median}/\varepsilon_{avg}$.

4 Conclusions

The shear rates of centrifugal separator inlets were found to be considerable, and depending on geometry and rotational speed they vary within a wide range. Thus, flocculation breakup may follow. However, the shear rate may also be substantially lowered using suitably well-designed inlets. In this way, also the flocculated particle clusters are more likely to remain intact and thereby improve the separation efficiency in downstream separation zones.

An analysis of the flow pattern and its pertinent properties, viz. energy dissipation rate, flow rate, and viscosity, gave further rudimentary relationships which with empirical corrections obtained may be used for estimating the remaining flocculation size passing through a shear zone.

By combining Eqs. (4), (5), and (9), an expression for the floc diameter of an inlet can be formulated as:

$$d_{avg} = C_f \left(\frac{C_{inlet} Q^2 \omega}{D_{inlet}^4 \nu} \right)^{-\gamma/2} \tag{10}$$

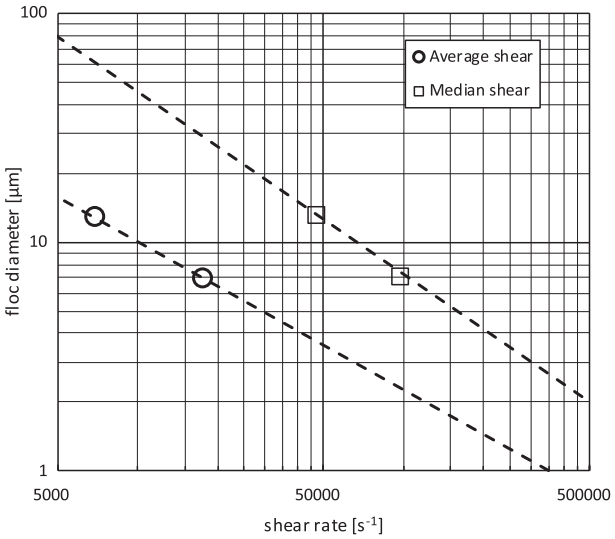

Figure 10. Fit of Eq. (4) to the data from [15].

With a known N_p, the average shear stress in the SDD can be calculated from Eqs. (5) and (7) as

$$G_{avg} = \left(\frac{N_p n^3 D_i^5}{\nu V}\right)^{1/2} \tag{11}$$

and used together with measured size distributions from the SDD for estimating C_f and γ. C_{inlet} can be determined from CFD simulations of the actual inlet or in lack of simulation data be set to 0.034 as a best guess for a hermetic inlet.

Acknowledgment

Dr. Tobias Merkel, BASF, is gratefully acknowledged for sharing the data from the spinning disc experiments. The research project received funding from the European Community's Framework Program for Research and Innovation Horizon 2020 (2014–2020) under grant agreement no. 637077.

The authors have declared no conflict of interest.

Symbols used

C_b	[–]	coefficient in droplet breakage correlation
C_f	[–]	floc strength coefficient
C_{inlet}	[–]	inlet shear coefficient
d_{avg}	[m]	floc diameter calculated using volume averages
d_{floc}	[m]	floc perimeter diameter
D_i	[m]	impeller diameter
D_{inlet}	[m]	inlet pipe diameter
d_m	[m]	floc diameter calculated using streamline median
d_{max}	[m]	maximum droplet diameter
g	[m s^{-2}]	gravitational acceleration
G_{avg}	[s^{-1}]	average rate of shear
n	[s^{-1}]	impeller rotation rate
N_p	[–]	impeller power number
P	[kg m^{2}s^{-3}]	power
Q	[m^{3}s^{-1}]	volumetric flow rate
V	[m^3]	volume
v_g	[m s^{-1}]	Stokes settling velocity

Greek letters

ε	[m^{2}s^{-3}]	energy dissipation rate per unit mass
ε_{avg}	[m^{2}s^{-3}]	volume average energy dissipation rate per unit mass
ε_{median}	[m^{2}s^{-3}]	streamline median energy dissipation rate per unit mass
γ	[–]	floc size exponent
μ	[kg m^{-1}s^{-1}]	fluid dynamic viscosity
ν	[m^{2}s^{-1}]	fluid kinematic viscosity
ω	[rad s^{-1}]	angular velocity
ρ	[kg m^{-3}]	fluid density
ρ_{floc}	[kg m^{-3}]	floc density
Σ	[m^2]	centrifuge area equivalent size
σ	[kg s^{-2}]	surface tension coefficient
τ	[kg m^{-2}s^{-2}]	torque

Abbreviations

CFD	computational fluid dynamics
SDD	spinning disc device

References

[1] C. M. Ambler, *J. Biochem. Microbiol. Technol. Eng.* **1959**, *1 (2)*, 185–205.
[2] H. Axelsson, B. Madsen, in *Ullmann's Encyclopedia of Industrial Chemistry*, Wiley-VCH Verlag, Weinheim **2006**.
[3] M. Boychyn, S. S. S. Yim, P. Ayazi Shamlou, M. Bulmer, J. More, M. Hoare, *Chem. Eng. Sci.* **2001**, *56*, 4759–4770.
[4] M. Boychyn, S. S. S. Yim, M. Bulmer, J. More, D. G. Bracewell, M. Hoare, *Bioprocess Biosyst. Eng.* **2004**, *26*, 385–391.
[5] N. Hutchinson, N. Bingham, N. Murrel, S. Farid, M. Hoare, *Biotechnol. Bioeng.* **2006**, 483–491.
[6] P. Jarvis, B. Jefferson, J. Gregory, S. A. Parsons, *Water Res.* **2005**, *39*, 3121–3137.
[7] J. O. Hinze, *AIChE J.* **1955**, *1 (3)*, 289–295.
[8] D. Parker, W. Kaufman, D. Jenkins, *J. Sanitary Eng. Div.* **1972**, *98*, 79–99.
[9] H. Tennekes, J. L. Lumley, *A First Course in Turbulence*, MIT-Press, Cambridge, MA **1972**.
[10] F. R. Menter, *AIAA 24th Fluid Dynamics Conf.*, Orlando, FL, July **1993**.
[11] F. Moukalled, L. Mangani, M. Darwish, *The Finite Volume Method in Computational Fluid Dynamics*, Springer International Publishing, New York **2016**.
[12] J. P. V. Doormaal, G. D. Raithby, *Numer. Heat Transfer* **1984**, *7 (2)*, 147–163.
[13] F. Menter, T. Esch, *16th Brazilian Congress of Mechanical Engineering*, Uberlândia, November **2001**.

[14] M. S. Levy, I. J. Collins, S. S. S. Yim, J. M. Ward, N. Titchener-Hooker, P. Ayazi Shamlou, P. Dunnill, *Bioprocess Eng.* **1999**, *20 (1)*, 7–13.

[15] T. Merkel, O. Blättler, S. Königsson, *Chem. Eng. Technol.* **2018**, *41*, in press.

[16] H. P. Greenspan, *The Theory of Rotating Fluids*, Breukelen Press, Brookline, MA **1990**.

